Local origin of the pseudogap in the attractive Hubbard model

Robert Peters[1,*] and Johannes Bauer[2,†]
[1]*Computational Condensed Matter Physics Laboratory, RIKEN, Wako, Saitama 351-0198, Japan*
[2]*Department of Physics, Harvard University, Cambridge, Massachusetts 02138, USA*
(Received 13 March 2015; published 22 July 2015)

We provide a fresh perspective on the pseudogap physics for attractive fermions as described by the three-dimensional Hubbard model. The pseudogap in the single-particle spectral function, which occurs for temperatures above the critical temperature T_c of the superfluid transition, is often interpreted in terms of preformed uncondensed pairs. Here we show that the occurrence of pseudogap physics can be consistently understood as due to local excitations which lead to a splitting of the quasiparticle peak for sufficiently large interaction. This effect becomes prominent at intermediate and high temperatures when the quantum-mechanical hopping is incoherent. We demonstrate the absence of the conjectured pairing temperature below which pseudogap physics is expected to occur. Our results are based on approximating the physics of the three-dimensional Hubbard model by dynamical mean-field theory calculations and a momentum independent self-energy. Our predictions can be tested with ultracold atoms in optical lattices with currently available temperatures and spectroscopic techniques.

DOI: 10.1103/PhysRevB.92.014511 PACS number(s): 74.20.−z, 74.25.Dw, 74.25.Gz, 71.10.Fd

I. INTRODUCTION

The analysis of peaks in the single-particle spectral function, measured, for instance, by photoemission experiments in solids or radio frequency (rf) spectroscopy for ultracold atoms, provides important information about correlation effects in interacting quantum many-body systems. In the limit of weak interactions the spectral function displays peaks close to the energies of the free fermion energy-momentum distribution and as such directly represents single-particle properties. At finite temperature and energies away from the Fermi surface, peaks are broadened and the width is indicative of interaction effects, which open up decay channels. If spontaneous symmetry breaking occurs below a certain temperature, such as in a superconductor below T_c, the single-particle excitations become gapped out and shifted by an amount Δ, the superconducting gap.

A more peculiar behavior is that of excitations being gapped out (or suppressed) even though no obvious symmetry breaking and thermodynamic ordering transition occurs. This is often referred to as pseudogap (PG) physics. The spectral gap can look very similar to a gap due to symmetry breaking at finite temperature. Therefore, it can be difficult to clarify the origin of PG physics and to distinguish whether it is due to some hidden order or a different effect. A very prominent example of such physics is provided by the experimental observations in the hole doped copper-oxide high-temperature superconductors [1,2], where a relatively large part of the phase diagram is occupied by such a PG behavior. This phenomenon has attracted an enormous amount of attention, however there is currently no consensus about the physical origin of the this PG for the cuprates, and different scenarios have been invoked as an explanation. These include hidden order [3], spin fluctuations [4], phase fluctuations and preformed pairs [5,6], and the interplay with charge fluctuations [7].

Here we focus on a conceptually simpler situation where PG physics has also been reported, and that is for systems of fermions with locally attractive interactions. In situations without nesting the dominant instability at low temperature is superconductivity and, correspondingly, pairing processes are expected to be most relevant. In particular, the crossover from weak-coupling Bardeen, Cooper, and Schrieffer [8] (BCS) theory of superconductivity to strong-coupling Bose-Einstein condensation (BEC) of pairs has been studied extensively and is a classical problem in condensed-matter physics [9–12]. In the last decade it has attracted renewed interest due to experimental realizations with ultracold fermions. Superfluidity has been reported in such systems [13–16], also in the case where the fermions are confined to an optical lattice [17]. Moreover, based on rf spectroscopy, PG signatures have been reported for two- [18] and three-dimensional systems without optical lattices [19–21].

Three nonexclusive concepts are usually invoked to discuss the origin of PG physics for attractive fermions.

(i) Preformed pairs: For intermediate coupling strength, pair formation without condensation is expected to occur at a certain temperature T_p which is larger than the superfluid (SF) phase transition temperature T_c. These preformed pairs can lead to PG formation as a certain binding energy is required to break the pair and resolve a single fermion excitation [12,20,22]. This idea leads to a popular scenario for PG physics and is illustrated in a schematic phase diagram in Fig. 1.

(ii) Pairing fluctuations above T_c and their effect on single-particle properties via a many-body self-energy can lead to PG physics [22].

(iii) Phase fluctuations: In a situation where fermions are paired one can imagine that a finite magnitude of the order parameter establishes locally, however no macroscopic coherent SF phase develops due to strong phase fluctuation [5]. In this situation the presence of the ordering tendency related to a gap can then lead to PG signatures in the spectral functions [23]. This behavior, which coincides with a small SF stiffness, is expected to be particularly pronounced in two-dimensional systems.

Within one and the same calculation it is very difficult to obtain nonperturbative results *and* to include all relevant

*robert.peters@riken.jp
†jbauer@physics.harvard.edu

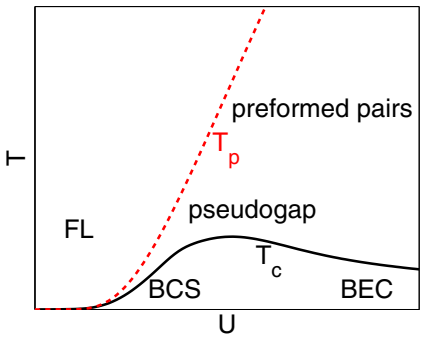

FIG. 1. (Color online) Schematic phase diagram for the preformed pair scenario in the T-U plane with critical temperature T_c, pairing temperature T_p, Fermi-liquid (FL) regime, and PG physics below T_p (after Randeria [20]).

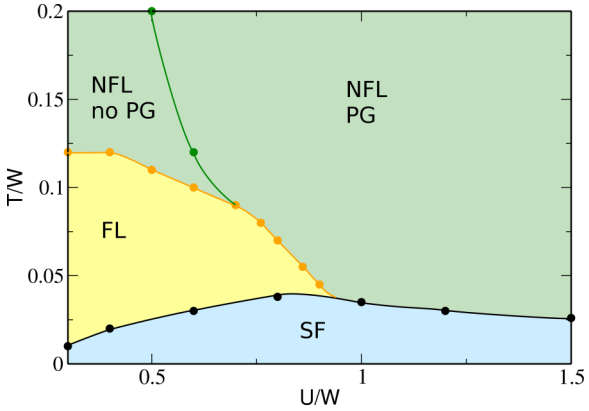

FIG. 2. (Color online) Phase diagram at half filling. We distinguish four different regimes: the superfluid phase (SF); a non-Fermi-liquid regime (NFL), which is separated into a region with PG in $\rho(\omega)$ and a region without PG (no PG); and a Fermi-liquid regime (FL) below the temperature T_{FL}.

fluctuation effects. The purpose of this work is to contribute to a better understanding of the importance of particular effects in the lattice situation based on nonperturbative calculations. It is important to distinguish different setups when comparing the occurrence of PG physics for attractive fermions. First of all, dimensionality plays an important role in determining the strength of fluctuations, and in particular the two-dimensional situation has more pronounced fluctuation effects. Moreover, results can differ in calculations for a model defined in the continuum and one on a lattice, such as the Hubbard model. A well-known example is the T_c curve which drops with the coupling strength on the lattice as $1/U$, whereas it approaches a constant in the continuum. Here we will analyze the attractive Hubbard model in three spatial dimensions. We will use the dynamical mean-field theory (DMFT) approximation [24] to compute the self-energies and spectral function in the normal and SF phase. This approximation is nonperturbative in the interaction strength and therefore can describe very well the occurrence of preformed pairs. However, it does not include the effect of phase fluctuations (iii) and also does not include the effect of small momentum pairing fluctuations. The PG physics observed in our work can therefore not be related to such effects. Phase fluctuations above T_c are usually argued to be of minor importance for spectral properties in three dimensions.

There is a substantial literature of previous work on BCS-BEC crossover and PG physics for attractive fermions, which however does not provide a clear and complete picture about PG physics. A popular approach is the diagrammatic T-matrix approximation [22,25,26], which captures well the effect of pairing fluctuations (ii). It was applied to the two-dimensional Hubbard model [27,28] and PG features have been found in the *non*-self-consistent version [22], also in the continuum in two [29] and three dimensions [30–32]. Self-consistent T-matrix calculations for the three-dimensional continuum model have found no PG in the spectrum [33,34]. However, in the two-dimensional case recently PG behavior was found [35]. There are also nonperturbative calculations, such as DMFT and quantum Monte Carlo (QMC), which found a PG features in the continuum model [36–38] and for the Hubbard model at different filling factors [39–45]. The latter results were found to be in good agreement with a diagrammatic technique [46]. It is worth noting that QMC techniques usually need to perform analytic continuation of imaginary axis data which can lead to uncertainties in results for spectral functions. DMFT studies, including cellular versions, for the attractive Hubbard model have been carried out in the normal phase [47–50], and in the broken symmetry phase [43,44,51–55].

Our major results are the following.

(1) For large enough coupling strength we find PG physics at temperatures $T > T_c$. At half filling the PG remains for *all* temperatures above T_c and therefore a pairing temperature T_p (Fig. 1) is not decisive to invoke the PG in the spectral function (see Fig. 2). For different fillings the spectral function is shifted due to the flattening of the Fermi function, such that the main suppression of spectral weight does not occur at $\omega = 0$.

(2) The occurrence of PG physics at high temperatures can be understood via local excitations on lattice sites visible for strong enough interactions.

(3) PG physics in the spectral function is related to non-Fermi-liquid (NFL) properties of the self-energy (see Fig. 3, detailed definition below).

(4) We demonstrate in detail how the PG transforms smoothly into the superconducting gap, when the temperature is lowered through T_c (see Fig. 6).

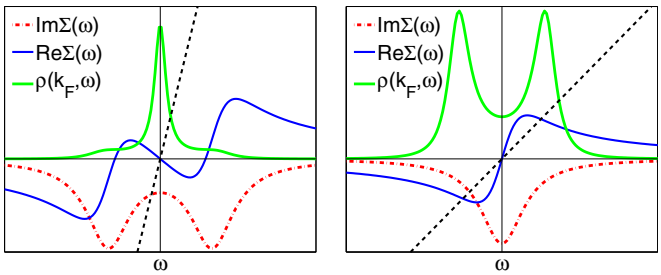

FIG. 3. (Color online) Schematic plot for real and imaginary parts of the self-energy $\Sigma(\omega)$ in the FL (left) and NFL (right) regime. We also show the corresponding spectral function $\rho(\boldsymbol{k}_F,\omega)$ which shows PG behavior in the NFL regime. The dashed diagonal line, ω, helps to identify the solutions of the equation $\omega = \mathrm{Re}\Sigma(\omega)$, and those positions roughly coincide with the PG peaks.

The paper is organized as follows: In Sec. II we briefly describe our model and method. Section III discusses conceptual background about the occurrence of PG physics in relation to the self-energy. In Secs. IV and V we show results for spectra and self-energies at and away from half filling before concluding in Sec. VI. In the Appendices we compare the DMFT-NRG calculations to iterated perturbation theory and to T-matrix calculations.

II. MODEL DEFINITION AND DMFT CALCULATIONS

Our study is based on the three-dimensional attractive Hubbard model [12,56–60], which in the grand canonical formalism reads

$$H = \sum_{i,j,\sigma}(t_{ij}c^{\dagger}_{i,\sigma}c_{j,\sigma} + \text{H.c.}) - \mu\sum_{i\sigma} n_{i\sigma} - U\sum_{i} n_{i,\uparrow}n_{i,\downarrow}, \tag{1}$$

with the chemical potential μ, the interaction strength $U > 0$, and the hopping parameters t_{ij}. $c^{\dagger}_{i,\sigma}$ creates a fermion at site i with spin σ, and $n_{i,\sigma} = c^{\dagger}_{i,\sigma}c_{i,\sigma}$. We take only a nearest-neighbor hopping $(-t)$, so that the noninteracting energy-dispersion relation in the three-dimensional cubic system is given as, $\boldsymbol{k} = (k_x,k_y,k_z)$,

$$\varepsilon_{\boldsymbol{k}} = -2t[\cos(k_x) + \cos(k_y) + \cos(k_z)]. \tag{2}$$

The dispersion satisfies $\varepsilon_{-\boldsymbol{k}} = \varepsilon_{\boldsymbol{k}}$. The corresponding density of states (DOS) is denoted by $\rho_0(\varepsilon)$. In the calculations we will use the hopping t and the bandwidth $W = 12t$ as energy scales.

The main method used to study the Hamiltonian (1) is the dynamical mean-field theory (DMFT) [24]. Within DMFT, we have to self-consistently solve a quantum impurity model describing a single lattice site in the environment of all other lattice sites. In order to calculate the self-energy for this quantum impurity model, we mainly use the numerical renormalization group (NRG) [61], which is able to calculate accurately expectation values, Green's functions, and self-energies at zero and finite temperatures [62,63] also in the superconducting case [54,55]. Dynamical correlation functions are calculated within the NRG by broadening of a large number of discrete excitations in the Lehman representation, and as such do not require analytic continuation. For our calculations, we choose a log-normal broadening function [61,64] with unusually narrow and temperature-independent width, $b = 0.3$. One of the main reasons for this is to avoid a large transfer of spectral weight to high energies which can be particularly important at higher temperatures. Using this narrow broadening leads to artificial oscillations in the spectra, which originate from the discretization of the bath in the NRG calculation. In order to produce physical spectra, we finally smooth these oscillations by averaging over $\Delta\omega = 0.01W$. This averaging is justified for the present purpose, because we do not expect very fine and sharp structures in our spectra on this energy scale to determine the physics of the PG. Furthermore, we carefully compared our NRG calculated spectra with iterated perturbation theory (see the Appendices). The latter technique does not require us to broaden discrete excitations and provides therefore a useful test in a suitable parameter regime.

III. FEATURES OF THE SPECTRAL FUNCTIONS AND SELF-ENERGY

Before presenting the results of our calculations it is useful to discuss some basic features of the Green's functions and self-energy, which will help us to better understand under which conditions PG physics occurs. In the literature PG physics is considered quite generally either for the integrated spectral function $\rho(\omega) = \frac{1}{N}\sum_{\boldsymbol{k}}\rho_{\boldsymbol{k}}(\omega)$, which is equivalent to the local spectrum $\rho_{ii}(\omega)$, or for $\boldsymbol{k}$-resolved spectra $\rho_{\boldsymbol{k}}(\omega)$ close to the Fermi surface. We will consider both quantities in this paper. We note that a PG in one of these does not necessarily imply one in the other quantity.

Let us first note that in the limit of high temperature $T \gg W,U$ correlation lengths become small and the physics is dominated by local processes [65]. This is seen, for instance, when we consider the bare single-particle propagator in imaginary time:

$$G^0_{ij}(\tau) = -\frac{1}{N}\sum_{\boldsymbol{k}} e^{i\boldsymbol{k}\boldsymbol{r}_{ij}}e^{-\xi_{\boldsymbol{k}}\tau}e^{\beta\xi_{\boldsymbol{k}}}n_{\mathrm{F}}(\xi_{\boldsymbol{k}}), \tag{3}$$

where $\xi_{\boldsymbol{k}} = \varepsilon_{\boldsymbol{k}} - \mu$ and $\tau \in [0,\beta)$. In the limit of high temperature, $\beta = 1/T \to 0$ and $n_{\mathrm{F}}(\xi_{\boldsymbol{k}}) \to 1/2$. Then $G^0_{ij}(\tau)$ in Eq. (3) becomes essentially local, $\sim\delta_{ij}$, and spatial components with $i \neq j$ vanish exponentially with length scale $\lambda \sim \frac{at}{T}$ [66]. Quantum-mechanical hopping is largely incoherent in this situation. This also means that DMFT based on a local self-consistent approximation can become very accurate in this high-temperature limit. For instance, high-temperature expansions for the three-dimensional Hubbard model agree well with DMFT calculations for thermodynamical quantities, and this remains the case down to temperatures of the order $T \simeq W/8$ [65,67]. One should, however, note that the self-energy of the three-dimensional Hubbard model does not become completely $\boldsymbol{k}$ independent even in the limit $T \to \infty$ [68].

What are the implications from this for the spectral function and the self-energy? The excitations in the limit where local physics dominates are determined by the local part of the Hamiltonian, $H_{\mathrm{loc}} = -\mu\sum_{i\sigma} n_{i\sigma} - U\sum_i n_{i,\uparrow}n_{i,\downarrow}$. At half filling the chemical potential is fixed to $\mu = -U/2$, and depending on the occupation $n = 0,1,2$ we have the energies $E_\alpha = 0,U/2,0$, respectively. Excitations in the spectral function have finite matrix elements for states where the particle number differs by one. Hence, in the spectral function excitation at energies $\Delta E = \pm U/2$ can be expected. The corresponding self-energy for the atomic problem reads $\Sigma_{ii}(\omega) = \frac{U^2}{4(\omega+i\Gamma)}$, where $\Gamma \to 0$. This implies δ-function peaks at $\pm U/2$ in the spectral function. In Sec. IV we will see that DMFT results at high temperature and large U are indeed of a similar form, $\mathrm{Im}\Sigma_{ii}(\omega) = -\frac{U^2\Gamma}{4(\omega^2+\Gamma^2)}$. Away from half filling the situation is more complicated, but similar features remain visible. If the peak in the self-energy is strong enough, we find in the spectral function increased weight at $\omega = \pm U/2$ and a suppression of spectral weight at the Fermi energy. These are the signatures of the PG in the integrated spectral function. For strong interactions this effect remains observable down to intermediate temperatures. In other words, the PG in $\rho(\omega)$ is related to the existence of Hubbard bands which are visible in the spectral function at all temperatures.

We now discuss the appearance of a gap and PG in the momentum resolved spectral function $\rho_{\boldsymbol{k}}(\omega)$. In the normal phase the Matsubara Green's function reads

$$G_{\boldsymbol{k}}(i\omega_n) = \frac{1}{i\omega_n - \xi_{\boldsymbol{k}} - \Sigma(i\omega_n)}, \tag{4}$$

where we have assumed a momentum independent self-energy as appropriate for DMFT calculations. The spectral function is obtained from analytic continuation, $i\omega_n \to \omega + i\eta$, $\eta \to 0$, to yield

$$\rho_{\boldsymbol{k}}(\omega) = -\frac{1}{\pi}\frac{\Sigma^I(\omega)}{[\omega - \xi_{\boldsymbol{k}} - \Sigma^R(\omega)]^2 + \Sigma^I(\omega)^2}. \tag{5}$$

We have separated real (R) and imaginary (I) parts of the self-energy.

In the SF state we can include an explicit symmetry-breaking term, Δ^0_{sc}, $\Delta^0_{\mathrm{sc}} \to 0$ for spontaneous symmetry breaking, and the noninteracting Green's-function matrix $\underline{G}^0_{\boldsymbol{k}}(i\omega_n)$ has the form

$$\underline{G}^0_{\boldsymbol{k}}(i\omega_n)^{-1} = \begin{pmatrix} i\omega_n - \xi_{\boldsymbol{k}} & \Delta^0_{\mathrm{sc}} \\ \Delta^0_{\mathrm{sc}} & i\omega_n + \xi_{\boldsymbol{k}} \end{pmatrix}. \tag{6}$$

For the interacting system we introduce the matrix self-energy $\underline{\Sigma}_{\boldsymbol{k}}(i\omega_n)$ such that the inverse of the full Green's-function matrix $\underline{G}_{\boldsymbol{k}}(i\omega_n)$ is given by the Dyson equation:

$$\underline{G}_{\boldsymbol{k}}(i\omega_n)^{-1} = \underline{G}^0_{\boldsymbol{k}}(i\omega_n)^{-1} - \underline{\Sigma}_{\boldsymbol{k}}(i\omega_n). \tag{7}$$

The diagonal component of the $\boldsymbol{k}$-dependent Green's function reads

$$G_{\boldsymbol{k}}(\omega) = \frac{\zeta_{2,\boldsymbol{k}}(i\omega_n)}{\zeta_{1,\boldsymbol{k}}(i\omega_n)\zeta_{2,\boldsymbol{k}}(i\omega_n) - \Sigma_{12}(i\omega_n)\Sigma_{21}(i\omega_n)}, \tag{8}$$

with $\zeta_{1,\boldsymbol{k}}(i\omega_n) = \omega - \xi_{\boldsymbol{k}} - \Sigma_{11}(i\omega_n)$, $\zeta_{2,\boldsymbol{k}}(i\omega_n) = i\omega_n + \xi_{\boldsymbol{k}} - \Sigma_{22}(i\omega_n)$. The off-diagonal self-energy $\Sigma_{12}(\omega)$, in particular its real part, plays the role of a dynamic gap function, $\mathrm{Re}\Sigma_{12}(\omega) \sim \Delta$. Therefore, low-energy spectral excitations which correspond to $\omega = z[\xi_{\boldsymbol{k}} - \Sigma^R(0)]$ in the normal phase are shifted by the gap Δ to $\pm E_{\boldsymbol{k}} \sim \pm z\sqrt{[\xi_{\boldsymbol{k}} - \Sigma^R(0)]^2 + \Delta^2}$, where $z^{-1} = 1 - \partial_\omega \overline{\Sigma}^R_{11}(0)$ is the renormalization factor. Usually we associate the gap with a binding energy of pairs and hence we can interpret this energy shift as an energy required to break a pair and see a single-particle excitation.

We now discuss the occurrence of a PG for momenta close to the Fermi surface in the situation where no off-diagonal self-energy is present. Thus consider $\boldsymbol{k} = \boldsymbol{k}_{\mathrm{F}}$ (interacting Fermi surface) such that $\xi_{\boldsymbol{k}_{\mathrm{F}}} - \Sigma^R(0) = 0$ [69]. Then we can write

$$\rho_{\boldsymbol{k}_{\mathrm{F}}}(\omega) = -\frac{1}{\pi}\frac{\Sigma^I(\omega)}{[\omega - \overline{\Sigma}^R(\omega)]^2 + \Sigma^I(\omega)^2}, \tag{9}$$

where $\overline{\Sigma}^R(\omega) = \Sigma^R(\omega) - \Sigma^R(0)$. Provided that $\Sigma^I(\omega)$ does not vary rapidly, we expect $\rho_{\boldsymbol{k}_{\mathrm{F}}}(\omega)$ to be peaked when the implicit equation $\omega = \overline{\Sigma}^R(\omega)$ is satisfied. According to our definitions there is always a solution to this equation for $\omega = 0$. In a weakly interacting system at low temperature $|\Sigma^I(\omega)|$ usually has a local minimum at $\omega = 0$:

$$\mathrm{Im}\Sigma(\omega) = -a(T) - b\omega^2, \tag{10}$$

where $a(T) \to 0$ for $T \to 0$ and $a, b > 0$. By the Kramers-Kronig relation $\partial_\omega \overline{\Sigma}^R(0) < 0$ [see Fig. 3 (left)]. Then the only solution of $\omega = \overline{\Sigma}^R(\omega)$ is the one at $\omega = 0$. This is the Fermi-liquid peak in the spectral function at $\omega = 0$ with width $\sim z|\Sigma^I(0)|$ and weight z, where $z^{-1} = 1 - \partial_\omega \overline{\Sigma}^R(0)$. We define the low-energy behavior in Eq. (10) as the Fermi-liquid (FL) regime.

A PG is obtained with different behavior [70,71]. If $|\Sigma^I(\omega)|$ possesses a local maximum at $\omega = 0$,

$$\mathrm{Im}\Sigma(\omega) = -a(T) + b\omega^2, \tag{11}$$

then $\partial_\omega \overline{\Sigma}^R(0) > 0$. If the slope is large enough we will then encounter additional solutions of $\omega = \overline{\Sigma}^R(\omega)$ as can be easily seen graphically [see Fig. 3 (right)]. Whether this is the case depends on the interaction strength, filling fraction, and temperature. Since $|\Sigma^I(\omega)|$ is decreasing, we obtain a local minimum at $\omega = 0$ in the spectral function and broadened peaks at finite energies. This means that the original peak at $\omega = 0$ is split and hence we obtain a PG. Notice that a local maximum of $|\Sigma^I(\omega)|$ does not necessarily lead to a PG, if the self-energy is not large enough. In the following we call the low-energy behavior of Eq. (11) non-Fermi-liquid (NFL) behavior. As we have discussed above $|\Sigma^I(\omega)|$ is typically maximal at $\omega = 0$ at high temperature when the physics becomes dominated by local interactions. It is also directly visible in the phase-space factor appearing in the second-order perturbation theory in U (see the Appendices). Therefore, at high temperature we expect NFL behavior, and at low temperature we usually have FL behavior. We define the crossover scale as T_{FL}, i.e., where the behavior of $\Sigma^I(\omega)$ changes from Eq. (11) to Eq. (10). In this picture PG behavior in $\rho_{\boldsymbol{k}_{\mathrm{F}}}(\omega)$ occurs therefore as long as (i) U is large enough ($\sim W$) and (ii) $T > T_{\mathrm{FL}}(U)$. In particular, the PG is always present above T_c if $T_c > T_{\mathrm{FL}}(U)$.

IV. PG PHYSICS AT HALF FILLING

In this section we analyze results from the DMFT calculations for spectral functions and self-energies and focus on the situation at half filling. An overview of the different regimes as a function of U and T is shown in Fig. 2.

The phase diagram includes the SF phase and the regimes where the self-energy shows FL and NFL behavior as defined in Eqs. (10) and (11), respectively. By performing calculations suppressing the SF phase below T_c, we find that the boundary between FL and NFL regimes (not shown) is connected to the bipolaron transition at $T = 0$, which is equivalent to the Mott transition for repulsive interactions. The NFL regime in the phase diagram is separated into a region for stronger interactions, where we observe a PG in the integrated spectral function, and a region without PG (no PG) for weaker couplings.

In the upper panels of Fig. 4 we show the interacting local DOS $\rho(\omega)$. At weak coupling and intermediate temperatures, $\rho(\omega)$ very much resembles the noninteraction DOS, $\rho_0(\omega)$, and the small self-energy does not have a pronounced effect. Although $|\mathrm{Im}\Sigma|$ is peaked at the Fermi energy for $U = 0.4W$ at high temperatures, there is no PG structure in the DOS. In contrast, for larger interactions, $U/W = 0.6$ and 1, we

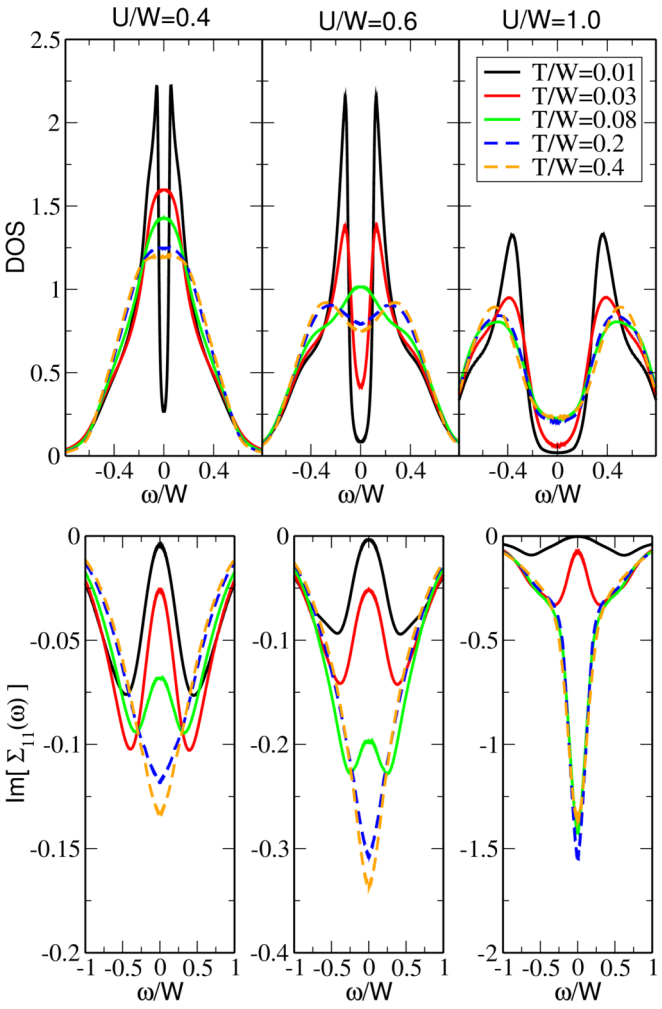

FIG. 4. (Color online) Integrated DOS, $\rho_{11}(\omega)$, and imaginary part of the self-energy, $\Sigma_{11}(\omega)$, for different interaction strengths and temperatures.

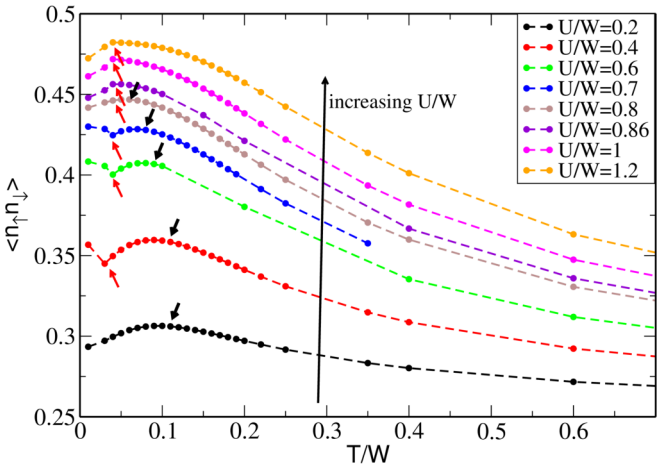

FIG. 5. (Color online) The local pair density $\langle n_\uparrow n_\downarrow \rangle$ for different temperatures and interaction strengths. The black arrow marks the transition from non-Fermi-liquid to Fermi-liquid behavior. The red arrow marks the transition into the SF phase.

find at high temperatures a PG structure of two peaks at $\pm U/2$ and a suppression of the density of states at $\omega = 0$. The behavior is more pronounced for larger interactions. In both cases the magnitude of the PG is clearly related to U. This structure is induced by the NFL peak in the $|\mathrm{Im}\Sigma|$ (lower panels). As discussed in Sec. III this result can be understood in terms of the local excitations dominating the physics at high temperature. At weak and intermediate interaction strengths the system crosses over to a FL regime before T_c is reached when decreasing the temperature. For $U/W = 0.4$ and 0.6, $|\mathrm{Im}\Sigma(\omega)|$ exhibits a dip at the Fermi energy at low enough temperature, $T/W < 0.1$, which is accompanied with a peak structure in the DOS. Such a change in the behavior of self-energy and DOS cannot be observed for strong coupling, where the PG structure exists for all temperatures above T_c. At very low temperatures, the system is in the SF phase in all cases, which is characterized by a gap in the DOS, which coincides with a dip in $\mathrm{Im}\Sigma(\omega)$. So even though the two cases, $U/W = 0.6$ and 1, in Fig. 4 look similar at high temperature (PG) and very low temperature (SF gap), they display a striking difference for intermediate temperatures. For the larger coupling strength the SF transition occurs from a PG state (see also Fig. 6); in contrast, for $U/W = 0.6$, the SF instability happens in the FL regime.

Further insights can be obtained by studying the behavior of the double occupancy or local pair density, $\langle n_\uparrow n_\downarrow \rangle$, which is shown in Fig. 5 for different temperatures and interaction strengths.

Independent of the interaction strength, in the high-temperature limit, $T \gg W, U$, the pair densities approach the noninteracting values n_σ^2, where n_σ is the density for one spin component, at half filling $\langle n_\uparrow n_\downarrow \rangle = 0.25$. In the atomic limit, $t = 0$, the double occupancy can be easily calculated. At half filling, all atomic states are occupied with equal probability, so that the double occupancy reads

$$\langle n_\uparrow n_\downarrow \rangle = \frac{1}{2 + 2\exp[-U/(2T)]}. \tag{12}$$

At high temperature, $T/W > 0.5$, this formula agrees very well with the results in Fig. 5, demonstrating again that the physics at high temperature is dominated by local processes.

Decreasing the temperature, $\langle n_\uparrow n_\downarrow \rangle$ increases due to the attractive interaction. This effect is stronger for stronger interaction. For interaction strengths $U/W < 0.8$, we find a maximum *before* the system enters the SF phase at T_c. This maximum appears to be correlated with the crossover temperature T_{FL} (black arrows) between FL and NFL behavior in the self-energy. The vanishing of the maximum in the pair density for interaction strengths $U/W > 0.8$ agrees with the vanishing of the FL regime phase in the phase diagram. For $U/W < 0.8$, the pair density decreases when lowering the temperature below T_{FL}, but then increases again when entering the SF phase (arrow at T_c). For strong interactions ($U/W > 0.8$) on the other hand, the pair density increases with decreasing temperature until T_c is reached and then decreases. This agrees with the known fact that the superfluidity is driven by interaction energy gain for weak coupling, as opposed to kinetic-energy gain for strongly coupled systems [53].

With these insights we can comment on how our results compare to the preformed pair scenario in Fig. 1. It is

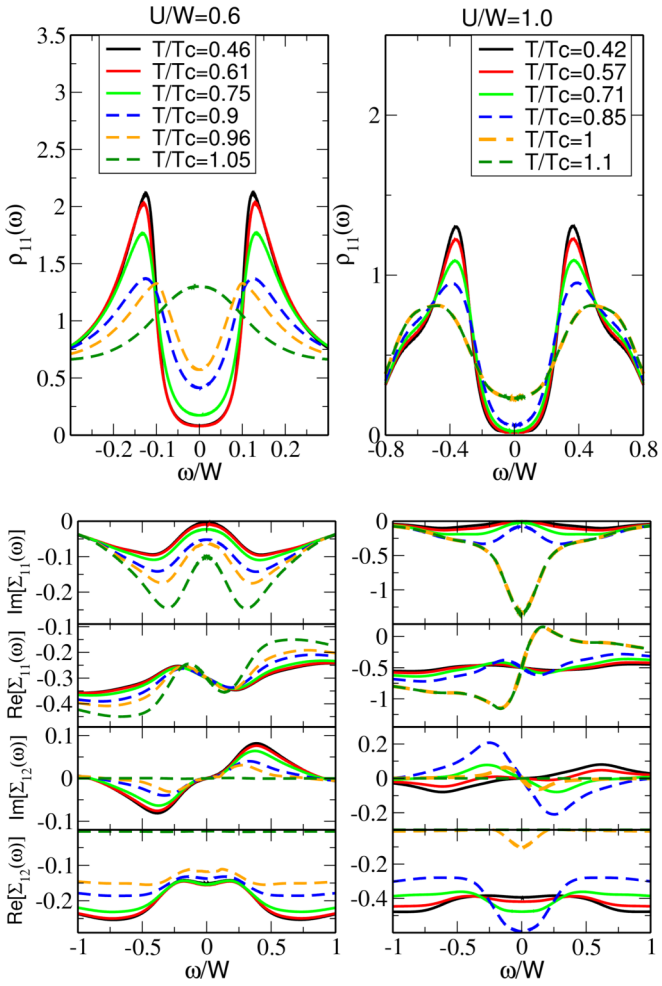

FIG. 6. (Color online) $\rho(\omega)$ and $\Sigma(\omega)$ close to the SF phase transition. We use the same legend for the self-energies as for the Green's functions. The transition temperatures are $T_c/W = 0.032$ for $U/W = 0.6$ and $T_c/W = 0.035$ for $U/W = 1.0$.

interesting to note that for very high temperatures the PG behavior in Fig. 4 does not change significantly anymore. In other words the PG persists and no T_p for its appearance can be identified. This is the case even for temperatures where the pair density has decreased to values close to the noninteracting result. Furthermore we found PG behavior for the two cases $U/W = 0.6$ and 1 at high temperature, but for intermediate temperatures ($T/W \sim 0.05$) the case $U/W = 0.6$ shows FL behavior. In both cases we observe a strongly enhanced local pair density for such temperatures, which can be interpreted as a preformed pair state, however the manifestation in the spectral function is different. Both of these observations are in clear contrast to the preformed pair scenario, where the existence of the PG behavior is linked to the presence of an enhanced pair density [20,22].

In Fig. 6, we take a closer look at dynamic response functions close to the SF transition temperature T_c.

The plots in the upper part of the figure show $\rho(\omega)$ for $U/W = 0.6$ and 1, which correspond to a transition into the SF phase from the FL and NFL regime, respectively. The lower part of the figure displays the corresponding diagonal and off-diagonal self-energies (real and imaginary parts). For the weaker-coupling case, $U/W = 0.6$, at $T > T_c$ there is the usual FL dip in $\mathrm{Im}\Sigma_{11}(\omega)$ and the corresponding peak in $\rho(\omega)$. When the temperature is lowered through T_c the off-diagonal self-energy becomes finite and a dip in $\rho(\omega)$ is induced. Very close below the transition temperature, the main effects for this come from $\mathrm{Re}\Sigma_{12}(\omega)$. Lowering the temperature further, the amplitude of the diagonal part of the self-energies decreases without showing new features. As discussed in Sec. III the gapping out of excitation is dominated by contributions from $\mathrm{Re}\Sigma_{12}(\omega)$.

In the case of stronger interaction, $U/W = 1$, superfluidity sets in the NFL regime with a PG at the Fermi energy. When lowering the temperature through T_c, the off-diagonal self-energy becomes finite, but at first the diagonal part of the self-energy remains nearly unchanged (the orange line, $T/T_c = 1$, overlaps with the dark green line, $T/T_c = 1.1$). On further reducing the temperature the off-diagonal self-energy increases substantially and $\mathrm{Im}\Sigma_{11}(\omega)$ is strongly reduced developing a FL dip at the Fermi energy. The gap in $\rho(\omega)$ changes smoothly from the PG with broad peaks separated by U to the sharper structures (coherence peaks) in the SF phase. It is interesting to note that the gap, if defined as the distance between the maxima, is larger above T_c in the PG regime than in the SF phase. One should also note that for low temperatures the gap becomes much more pronounced with a suppression of spectral weight at $\omega = 0$ and as such is approaching a full gap in the limit $T \to 0$.

A remarkable observation is that the qualitative behavior of the off-diagonal part of the self-energy can change within the SF phase. Generally, $|\mathrm{Re}\Sigma_{12}(\omega)|$ approaches the mean-field result $U\langle c_{i,\uparrow}c_{i,\downarrow}\rangle$ for $|\omega| \to \infty$ [55]. At weaker coupling ($U/W = 0.6$) and low temperature it is minimal for small ω. Decreasing the temperature, the anomalous expectation value increases and this is reflected in the results for $\Sigma_{12}(\omega)$. The ω dependence can be understood at weak coupling from the effective interaction for inducing superfluidity, which possesses a repulsive component which is peaked for small ω [72]. However, when entering the SF phase from the PG regime at stronger coupling ($U/W = 1$), $|\mathrm{Re}\Sigma_{12}(\omega)|$ first develops a strong maximum at $\omega = 0$. When the temperature is lowered further this behavior continually reverts to the one of the weak-coupling situation. The form of the spectral function changes at T_c and there is a shift from the gap feature being induced by $\Sigma_{11}(\omega)$ (above T_c) to $\Sigma_{12}(\omega)$ (below T_c). The observed strong changes are related to this shift and a more thorough understanding requires further investigation.

We now turn our attention to features in the momentum resolved spectral function $\rho_{\boldsymbol{k}}(\omega)$. A good overview of the behavior for different interactions and temperatures can be obtained in the intensity plots in Fig. 7.

We show $\rho_{\boldsymbol{k}}(\omega)$ for three interaction strengths [$U/W = 0.4$ (upper panels), 0.6 (middle panels), and 1 (lower panels)] for three different temperatures [$T/W = 0.2$ (left), 0.08 (middle), and 0.01 (right)]. We also show the Fermi level (dashed line) and the noninteracting dispersion (full red line) as an orientation. At weak coupling, $U/W = 0.4$, the spectral function only displays a weak modification from the noninteracting result with certain broadening of the peaks and a minor shift of spectral weight. At low temperature the system is SF and excitations at $\boldsymbol{k}_F$ are gapped out. Notice that the width

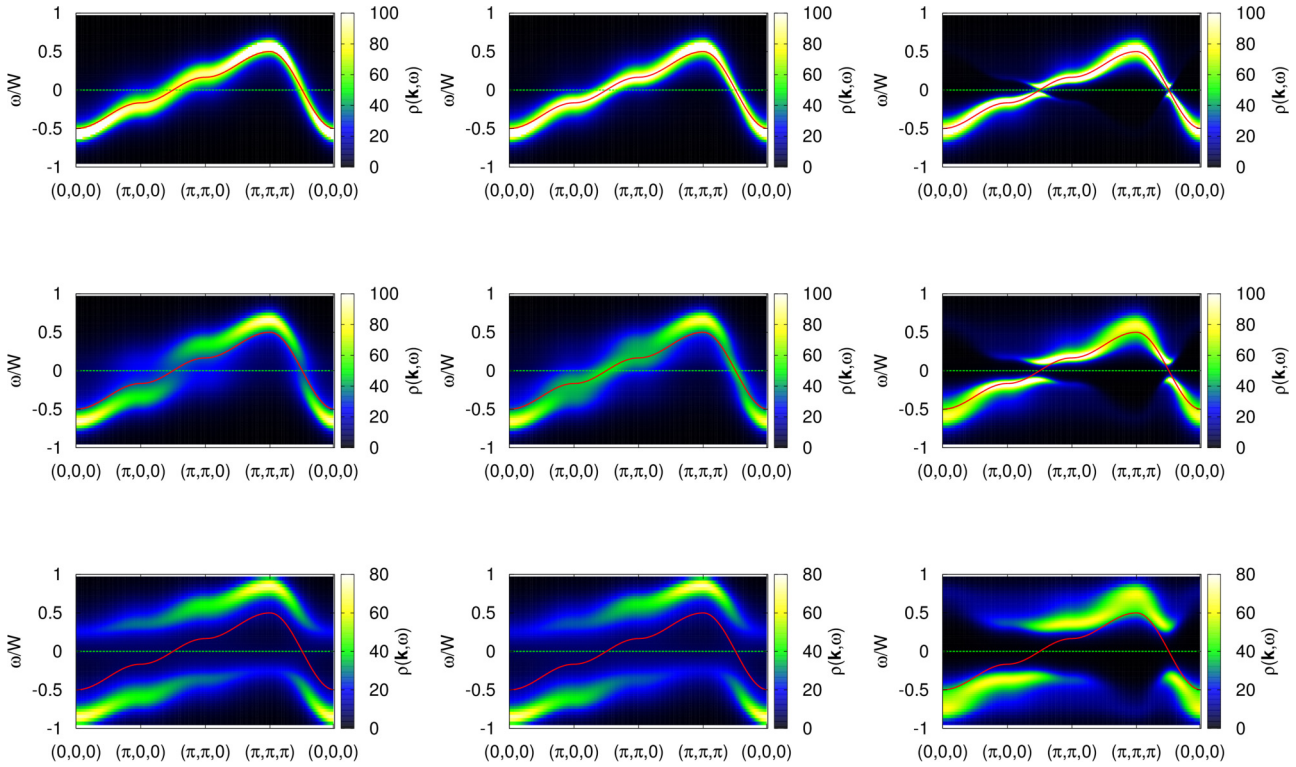

FIG. 7. (Color online) Momentum resolved spectral function for $U/W = 0.4$ (upper panel), $U/W = 0.6$ (middle panels), and $U/W = 1$ (lower panels). The temperatures are $T/W = 0.2, 0.08, 0.01$ from left to right. The red line corresponds to the noninteracting system; the green line corresponds to the Fermi energy.

of the Bogoliubov peaks at the gap edge is overestimated by our broadening procedure [55].

For $U/W = 0.6$, we find similar features for $\rho_{\boldsymbol{k}}(\omega)$ as what has been found for the integrated spectral function, $\rho(\omega)$, as far as the PG is concerned. At high temperatures we see a broadened dispersion similar to but shifted from the noninteracting one. Spectral weight is suppressed at the Fermi energy such that PG features are realized at high temperatures. Curiously, this PG closes at intermediated temperatures $\sim T_{\mathrm{FL}}$ where the behavior of the self-energy changes. Below T_c the spectrum is gapped again. Notice that band renormalization features appear somewhat weaker than at high temperatures.

For $U/W = 1$ the NFL regime extends from high temperatures down to T_c. The self-energy undergoes only very slight changes when decreasing the temperature in the NFL regime. Accordingly, the momentum resolved spectral functions for $T/W = 0.2$ and 0.08 (lower left panel and lower middle panel) are nearly the same. We observe a large PG around the Fermi energy; the spectral weight at the Fermi energy is very small. When entering the SF phase, gap features are visible and the dispersion changes in the vicinity of $\omega = 0$. For this interaction strength, we observe a clear deviation between the noninteracting band structure and the interacting spectral function. In the SF phase we find a mirror or "shadow" band appearing as reflected from $\omega = 0$. These bands can be understood due to a particle-hole doubling in the Nambu representation. This is an effect also observed in the antiferromagnetically ordered phase with zone doubling [73].

In Fig. 8 we show particular cuts for $\rho_{\boldsymbol{k}_{\mathrm{F}}}(\omega)$ as a function of ω. Here we can see the PG features even more clearly. Similar to the integrated spectrum, $\rho(\omega)$, the PG is absent for the weak-coupling case, $U/W = 0.4$, but present at high temperature for stronger interactions, $U/W = 0.6$ and 1. For $U/W = 0.6$ the PG disappears in the FL regime, whereas it remains for $U/W = 1$. We also show the real part of the diagonal self-energy. As discussed in Sec. III, the peak splitting in $\rho_{\boldsymbol{k}_{\mathrm{F}}}(\omega)$ can be induced from nontrivial solutions of $\omega = \mathrm{Re}\,\overline{\Sigma}_{11}(\omega)$, and we have included a dashed line to see this graphically. As can be clearly seen, this condition is not satisfied in the weak-coupling case. In contrast, at strong

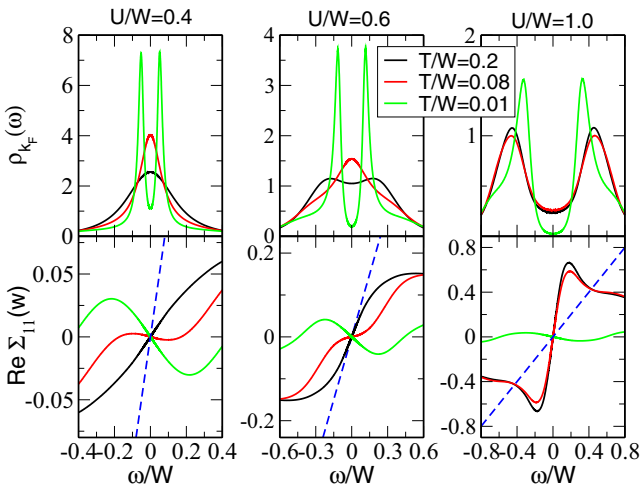

FIG. 8. (Color online) $\rho_{\boldsymbol{k}_{\mathrm{F}}}(\omega)$ for $\boldsymbol{k}_{\mathrm{F}} = (\pi/2, \pi/2, \pi/2)$ for $U/W = 0.4$, 0.6, and 1 for different temperatures.

coupling, $U/W = 1$, the intersection points characterize the peak positions well. The spectral function changes in the SF phase (lowest temperatures), where the coherence peaks at the gap edge become visible.

V. PG PHYSICS AWAY FROM HALF FILLING

So far we have focused on the situation at half filling where the discussion is somewhat simplified due to the particle-hole symmetry. In this section we show results for different filling factors ($n < 1$) to see how the PG behavior is affected. This is important for comparison with experiments with ultracold atoms, where due to the trapping potential no homogeneous filling fraction can be expected.

In Fig. 9 results for $\rho(\omega)$ and $\mathrm{Im}\Sigma(\omega)$ analogous to the ones in Fig. 4 for the half-filled case are displayed for $n = 0.5$ over a wide temperature range. The lowest temperature corresponds to a gapped SF state. Looking at the self-energies in the lower panel, we can clearly see that the classification into FL and NFL regions is still applicable and $|\mathrm{Im}\Sigma(\omega)|$ can either show a double peak with dip in the vicinity of $\omega = 0$ (FL) or a strong single peak (NFL). It is useful here to distinguish temperatures $T/W \lesssim 0.2$, where features are close to $\omega = 0$,

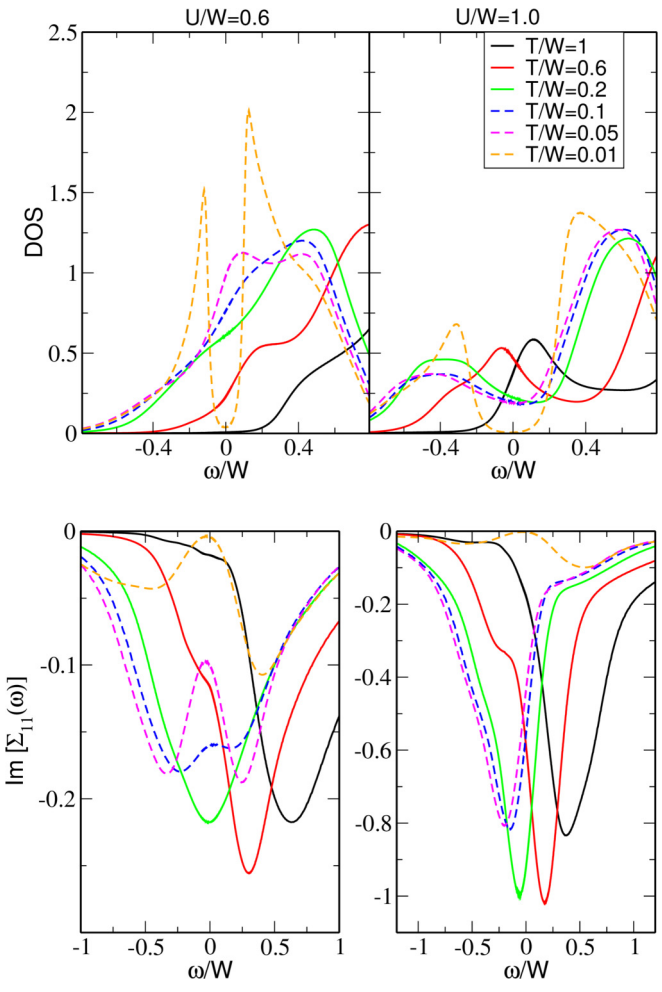

FIG. 9. (Color online) The DOS and imaginary part of the self-energy for $U/W = 0.6$ and 1 for different temperatures. The filling of the system is fixed to $n = 0.5$.

and higher temperatures, where the NFL peak in $|\mathrm{Im}\Sigma(\omega)|$ moves systematically to higher energies. In contrast to the half-filled situation the case $U/W = 0.6$ does not show a clear PG in $\rho(\omega)$. However, for $U/W = 1$ the PG is clearly visible. For lower temperatures the minimum in $\rho(\omega)$ is close to $\omega = 0$ and for higher temperatures it moves to higher energies together with the NFL peak in $|\mathrm{Im}\Sigma(\omega)|$. Notice, however, that the minimum in $\rho(\omega)$ and the peak in $|\mathrm{Im}\Sigma(\omega)|$ do not coincide as they do for $n = 1$. The shift of the PG with temperature can be understood by recalling that at high temperature the Fermi distribution becomes flatter such that higher energies contribute to the particle number, $n = \int d\omega \rho(\omega) n_F(\omega)$. To satisfy this relation at higher temperature the spectrum has to be shifted.

The PG structure in $\rho(\omega)$ at elevated temperature can still be understood from the local picture. For $n < 1$, we can write $\mu = -U/2 - \Delta\mu$ ($U > 0$) assuming $\Delta\mu > 0$, and the atomic energies are $E_\alpha = 0, U/2 + \Delta\mu, 2\Delta\mu$. The partition function reads

$$Z = 1 + 2e^{-\beta(U/2+\Delta\mu)} + e^{-\beta 2\Delta\mu}. \tag{13}$$

There are now excitations at $\omega_+ = U/2 + \Delta\mu$ and $\omega_- = -U/2 + \Delta\mu$ with generally asymmetric weights:

$$w_+ = \frac{1}{Z}[1 + e^{-\beta(U/2+\Delta\mu)}], \tag{14}$$

and

$$w_- = \frac{1}{Z}[e^{-\beta 2\Delta\mu} + e^{-\beta(U/2+\Delta\mu)}], \tag{15}$$

respectively.

Without showing explicit results we note that the pair density $\langle n_\uparrow n_\downarrow \rangle$ displays a similar temperature dependence for $n = 0.5$ to what was shown in Fig. 5, increasing from n_σ^2 at large T to larger values (maximal $n/2$). Therefore, similarly to the half-filled case PG behavior can coincide with an enhanced pair density for large interactions and $T_c \lesssim T$. However, we also find cases, e.g., $U/W = 0.6$, $T/W = 0.05$, with enhanced pair density ($\langle n_\uparrow n_\downarrow \rangle \approx 0.17$) and no PG behavior, in contrast to the expected relation in the preformed pair scenario.

In order to get an insight to overall trends, we compare several different fillings in Fig. 10. We show $\rho(\omega)$ and $\mathrm{Im}\Sigma(\omega)$ for $U/W = 0.6$ and 1 for low temperature, $T/W = 0.05$, in the normal phase. For $U/W = 0.6$ $\rho(\omega)$ exhibits a FL dip in $\mathrm{Im}\Sigma(\omega)$. It is clearly visible, even for $n = 0.1$, that the self-energy does not change its structure when reducing the filling further. The frequency dependence in this FL regime is relatively symmetric with respect to $\omega = 0$. The DOS, on the other hand, changes with n. While for $n = 0.5$ a clear peak close to the Fermi energy is visible in the DOS at low temperature, such a peak is hardly noticeable for $n = 0.2$, and it has disappeared for $n = 0.1$. The amplitude of the self-energy has become too weak to change the spectrum and we essentially see a shifted noninteracting DOS.

For $U/W = 1$, we find a NFL peak in $\mathrm{Im}\Sigma(\omega)$ for all fillings in Fig. 10. We observe similar effects as for weaker interactions when reducing the filling as far as the strength of the self-energy is concerned. However, we find a clear PG structure in the DOS. While the PG structure at low temperature is pinned to $\omega = 0$, at high temperature the whole spectrum including

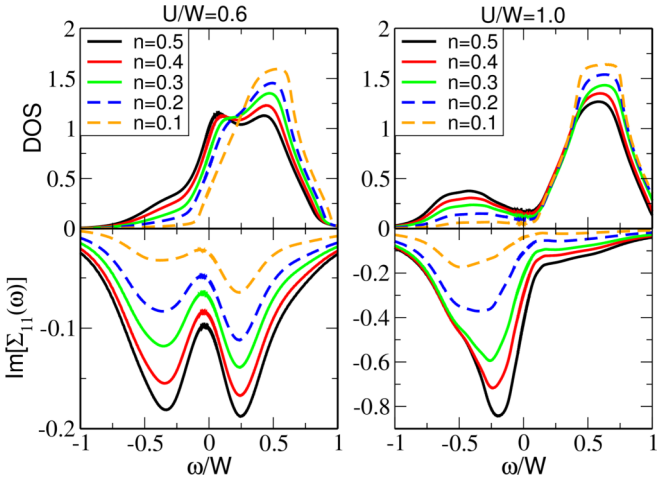

FIG. 10. (Color online) The DOS and imaginary part of the self-energy for $U/W = 0.6$ and 1 for different fillings. The temperature of the system is $T/W = 0.05$. All data shown correspond to the normal phase.

the PG is shifted to high frequencies (see Fig. 9). Note that at high temperature due to the flattening of $n_F(\omega)$ the Fermi energy ($\omega = 0$) does not play such an important role as it does for low temperatures.

In summary, when analyzing $\rho(\omega)$ and $\mathrm{Im}\Sigma(\omega)$ we can find similar features to the ones of the half-filled situation and a PG appears for suitable parameters. However, depending on filling, temperature, and interaction strength, the occurrence of the PG may be limited. At high temperatures it can be shifted away from $\omega = 0$, although it is still clearly visible in the spectrum. Moreover, the impact of the local Hubbard interaction becomes weaker for a system with a smaller filling factor.

Momentum resolved spectra for $n = 0.5$ and various values of T and U are displayed in Fig. 11. Generally, the features are similar to the half-filled case. For weak coupling ($U/W = 0.4$) we find a shifted and broadened spectrum which shows a SF gap at low temperature. For intermediate coupling ($U/W = 0.6$) interaction effects are more visible in the spectrum, resulting in stronger band renormalization effects and shifts of spectral weight. However, in contrast to $n = 1$ no clear PG becomes visible in $\rho_{\boldsymbol{k}}(\omega)$. For $U/W = 1$, we see strong interaction effects and PG features at all temperatures above T_c. We also clearly observe an asymmetry in the intensity, which is substantially lower for the $\omega < 0$ part of the spectrum.

Particular cuts along ω for momenta which satisfy $\xi_{\boldsymbol{k}_F} + \mathrm{Re}\Sigma(0) = 0$ are shown in Fig. 12. At weak coupling ($U/W = 0.4$) the FL peak is gapped out when the temperature is lowered below T_c. For intermediate coupling ($U/W = 0.6$) above T_c we find that the FL peak is shifted away from $\omega = 0$ to higher energies. Also the coherence peaks below T_c show some asymmetry due to self-energy effects. A clear PG is only visible for larger interactions, $U/W = 1$. The lower panel shows again the real part of the self-energy. In contrast to the situation at half filling, the peaks in $\rho_{\boldsymbol{k}_F}(\omega)$ are not well explained by the intersection, $\omega = \mathrm{Re}\overline{\Sigma}(\omega)$. In this situation the variation of $\mathrm{Im}\Sigma(\omega)$ is too strong, invalidating the simple arguments of Sec. III. Nevertheless a NFL peak form of the self-energy is clearly important for the PG behavior.

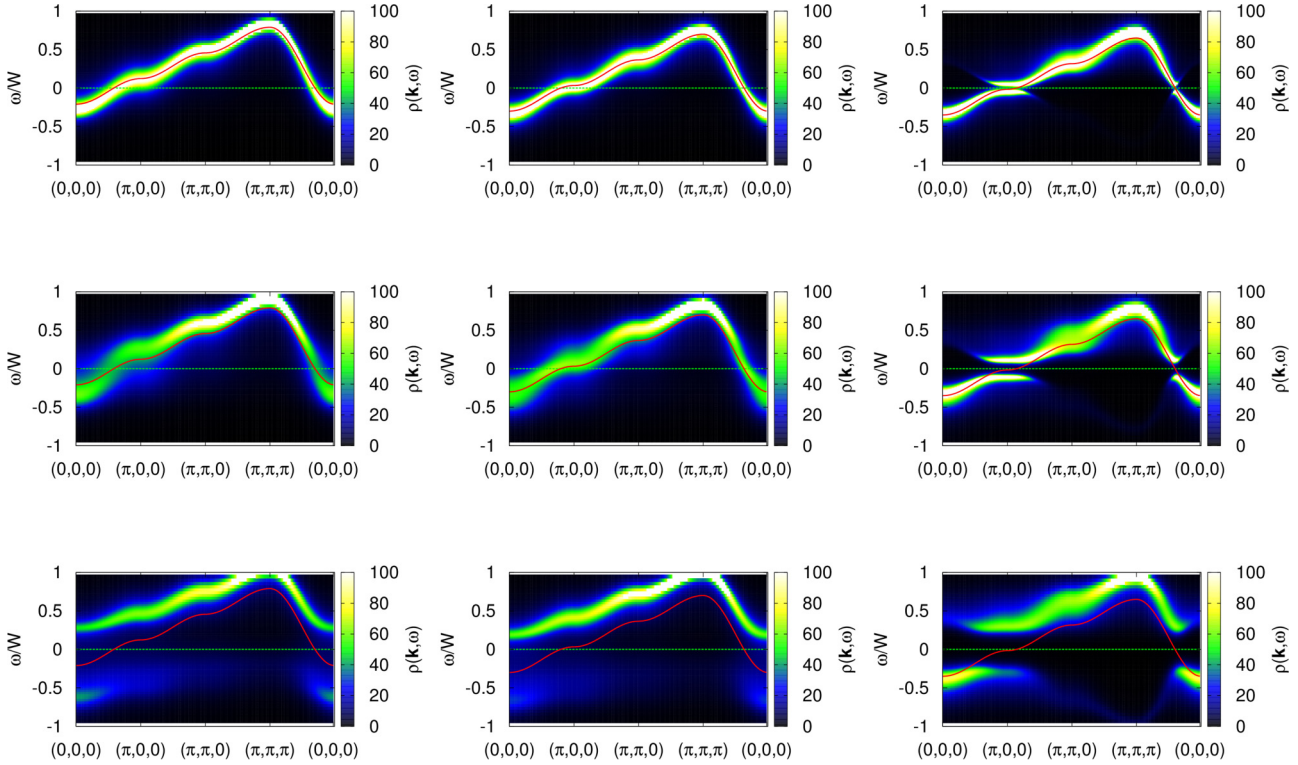

FIG. 11. (Color online) Momentum resolved spectral function $\rho_{\boldsymbol{k}}(\omega)$ for $n = 0.5$ from top to bottom—$U/W = 0.4$, 0.6, and 1—and from left to right—$T/W = 0.2$, 0.08, and 0.01. The red line corresponds to the noninteracting dispersion $\varepsilon_{\boldsymbol{k}}$; the dashed green line corresponds to the Fermi energy.

VI. DISCUSSION AND CONCLUSIONS

We have analyzed the occurrence of PG features in the integrated and $\boldsymbol{k}$-resolved spectral function of the three-dimensional attractive Hubbard model for different filling factors. Properties of the spectral functions have been traced back to the characteristic behavior of the self-energy. We find PG behavior as long as the interaction U is large enough ($\sim W$) and the self-energy shows NFL behavior, i.e., $T > T_{\mathrm{FL}}(U)$. Our results show marked deviation from the popular preformed pair scenario, where PG behavior is directly linked with the formation of pairs at a temperature T_{p}: (i) We find that PG behavior persists up to large temperatures and is not bounded by some temperature scale T_{p}, and (ii) we find cases with a substantially enhanced pair density where no PG behavior occurs. The first effect is related to the fact that we are working with a lattice model, such that local excitations are always well defined and related to μ and U. This might be different in the continuum where it is conceivable that the preformed pair scenario of Fig. 1 is applicable. On the other hand we expect the PG to be present at large temperatures as a nonperturbative local lattice effect also in the two-dimensional lattice model. Certainly, other effects like strong phase fluctuations and small momentum pairing fluctuations, not contained in our calculations, can lead to a substantial extension of the regimes where PG behavior occurs.

A word of caution is in order when discussing the large temperatures addressed in this paper. Here we dealt with a strict one-band model where the kinetic energy is limited by the bandwidth. In most real systems very high temperature would activate higher bands, and in solid-state systems it can lead to the melting of the crystal structure; such effects are obviously not allowed in our setup.

Experiments with ultracold atoms in optical lattices provide an excellent platform to test our predictions. Interactions can be tuned in a wide range by Feshbach resonances, the lattices can be loaded with different filling factors, and a temperature range $T/W = 0.1$–0.2 is routinely accessible. Integrated and momentum resolved spectra can be measured such that a direct comparison with our predictions is possible. Thus, we hope that our work will stimulate further efforts in this field which contribute to a better understanding of the intriguing PG physics.

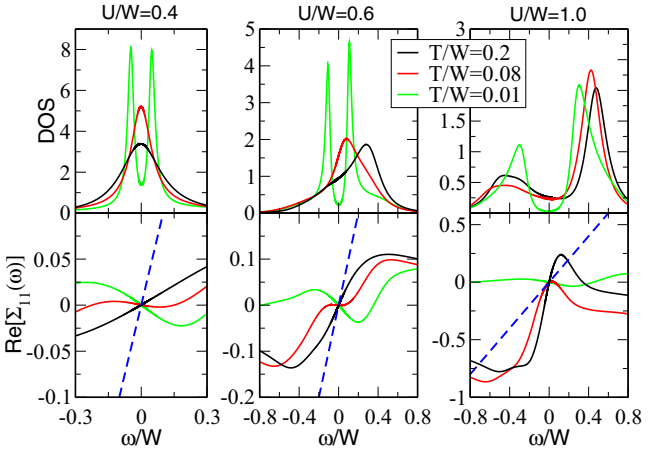

FIG. 12. (Color online) $\rho_{k_{\mathrm{F}}}(\omega)$ for $U/W = 0.4$, 0.6, and 1 and different temperatures. Notice that the lowest temperature $T/W = 0.01$ is below T_c in all cases. The lower panels show the real part of the self-energy including the line $y = \omega$.

ACKNOWLEDGMENTS

We wish to thank M. Capone, N. Dupuis, A. Georges, O. Gunnarsson, B. Halperin, W. Metzner, E. Perepelitsky, M. Punk, P. Strack, A. Toschi, and A. Koga for very helpful discussions and suggestions during different stages of this work. J.B. acknowledges financial support from the Deutsche Forschungsgemeinschaft through Grant No. BA 4371/1-1. R.P. is supported by the foreign postdoc researcher (FPR) program of RIKEN. Computer calculations have been done at the supercomputer facilities of RIKEN and the Kashiwa supercomputer of the Institute of Solid State Physics in Japan.

APPENDIX A: T-MATRIX APPROXIMATION

A popular approximation for the self-energy is the so-called T-matrix approximation, which corresponds essentially to summing the scattering processes in the particle-particle channel. One has [27,33]

$$\Sigma^{(1)} = TU \sum_{m,\boldsymbol{q}} e^{i\omega_m \eta} G(\boldsymbol{q}, i\omega_m), \tag{A1}$$

or equivalently

$$\Sigma^{(1)} = U \sum_{\boldsymbol{q}} \int \mathrm{d}\omega\ \rho(\boldsymbol{q},\omega) n_{\mathrm{F}}(\omega), \tag{A2}$$

and

$$\Sigma^{\mathrm{T}}_{\boldsymbol{k}}(i\omega_n) = T \sum_{m,\boldsymbol{q}} e^{i\omega_n \eta} \Gamma(\boldsymbol{q}, i\omega_m) G(\boldsymbol{q}-\boldsymbol{k}, i\omega_m - i\omega_n), \tag{A3}$$

with $\eta \to 0$. Here we defined

$$\Gamma(\boldsymbol{q}, i\omega_m) = \frac{U^2 K(\boldsymbol{q}, i\omega_m)}{1 - U K(\boldsymbol{q}, i\omega_m)}, \tag{A4}$$

with the particle-particle propagator:

$$K(\boldsymbol{q}, i\omega_m) = -T \sum_{n,\boldsymbol{q}} G(\boldsymbol{q}-\boldsymbol{k}, i\omega_m - i\omega_n) G(\boldsymbol{k}, i\omega_n). \tag{A5}$$

The self-energy is $\Sigma_{\boldsymbol{k}}(i\omega_n) = \Sigma^{(1)}_{\boldsymbol{k}}(i\omega_n) + \Sigma^{\mathrm{T}}_{\boldsymbol{k}}(i\omega_n)$.

In the local approximation, the expression simplifies. We find the following result after analytic continuation:

$$\Sigma^{(1)} = U \int \mathrm{d}\omega\ \rho_G(\omega) n_{\mathrm{F}}(\omega), \tag{A6}$$

and

$$\Sigma^{\mathrm{T}}(\omega) = \int \mathrm{d}\omega_1 \int \mathrm{d}\omega_2\ \frac{\rho_\Gamma(\omega_1)\rho_G(\omega_2)}{\omega^+ - \omega_1 + \omega_2} [n_{\mathrm{B}}(\omega_1) + n_{\mathrm{F}}(\omega_2)]. \tag{A7}$$

We have

$$K(i\omega_m) = -T \sum_n G(i\omega_m - i\omega_n) G(i\omega_n), \tag{A8}$$

and $\rho_\Gamma = -\frac{1}{\pi}\mathrm{Im}\Gamma(\omega^+)$. Introducing spectral functions we can also write

$$K(\omega^+) = \int d\omega_1 \int d\omega_2 \frac{\rho_G(\omega_1)\rho_G(\omega_2)}{\omega^+ - \omega_1 - \omega_2}[n_F(\omega_1) - n_F(-\omega_2)], \tag{A9}$$

and

$$\Gamma(i\omega_m) = \frac{U^2 K(i\omega_m)}{1 - UK(i\omega_m)}. \tag{A10}$$

The T-matrix calculations can be done non-self-consistently (Tnsc) and self-consistently (Tsc).

APPENDIX B: COMPARISON OF NRG-DMFT WITH IPT AND T MATRIX

We start with a comparison of the DMFT results obtained using NRG calculations for the effective impurity model with DMFT calculations using second-order perturbation theory, usually termed iterated perturbation theory (IPT). IPT gives qualitatively reliable results in the half-filled Hubbard model [24]. Since IPT does not require a prescription of broadening discrete excitations, this comparison helps to validate the finite temperature broadening procedure described in Sec. II. We focus on results at half filling in this section. In Fig. 13 we show a comparison of the imaginary part of the self-energy, $\mathrm{Im}\Sigma(\omega)$, and the integrated spectral function, $\rho(\omega)$, for $U/W = 0.6$ (left) and 1 (right) and different temperatures.

Overall the agreement is good with minor deviations in the tails. There is a particularly visible difference for $U/W = 1$, where the IPT result for $\mathrm{Im}\Sigma(\omega)$ shows a somewhat stronger peak. This leads to a more pronounced PG in $\rho(\omega)$. We conclude that the DMFT-NRG results at high temperatures have the qualitative correct form and the PG remains there.

We also provide a comparison of the DMFT-NRG results with T-matrix calculations. In particular, we use Eq. (A6) and following, and include self-consistent (Tsc) and non-self-consistent (Tnsc) results. Note that the T-matrix

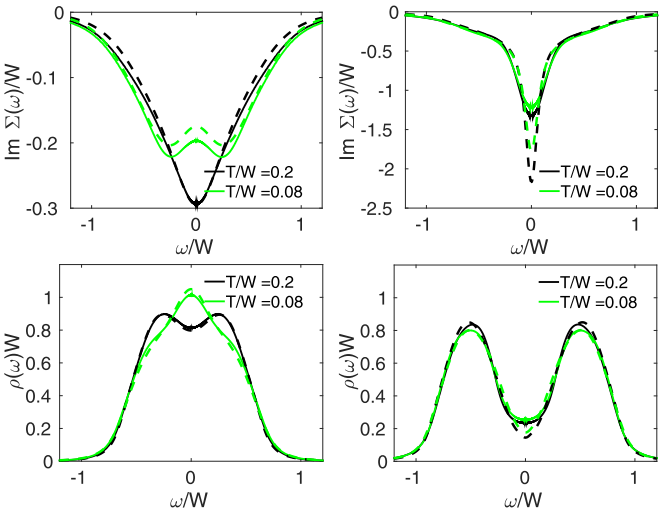

FIG. 13. (Color online) Comparison of DMFT-NRG (full lines) and IPT (dashed lines) results for $U/W = 0.6$ (left) and 1 (right) for $\mathrm{Im}\Sigma(\omega)$ and $\rho(\omega)$.

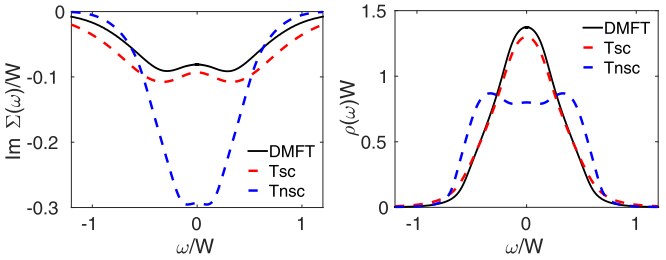

FIG. 14. (Color online) Comparison of DMFT-NRG result with self-consistent (Tsc) and non-self-consistent (Tnsc) T-matrix calculations for $\mathrm{Im}\Sigma(\omega)$ and $\rho(\omega)$ for $U/W = 0.4$ and $T/W = 0.1$.

calculations are only sensible as long as $1 - U\mathrm{Re}K(\omega)$ does not become zero, which is particularly important for the non-self-consistent case. At weak coupling ($U/W = 0.2$, not shown) one can find reasonable agreement of T-matrix calculations with the DMFT-NRG and all calculations give no PG behavior. However, in this situation also second-order perturbation theory gives satisfactory agreement.

As seen in Fig. 14 for $U/W = 0.4$ and $T/W = 0.1$, Tsc and DMFT still show reasonable agreement, whereas Tnsc calculations can lead to a strong overestimate for $\mathrm{Im}\Sigma(\omega)$. This can lead to a PG feature in $\rho(\omega)$, even though calculations with the DMFT-NRG give no PG behavior.

For intermediate coupling, $U/W = 0.6$, and $T/W = 0.2$, we show a further comparison in Fig. 15.

In this case both T-matrix calculations give unreliable results. The self-energy of the self-consistent version is too small and $\rho(\omega)$ shows no PG. The non-self-consistent calculation shows a PG but its magnitude is largely overestimated. For larger interactions, for instance, $U/W = 1$, the deviations get worse. We therefore conclude that T-matrix calculations—both self-consistent and non-self-consistent—within the local approximation do not give reliable results for the PG physics of the three-dimensional Hubbard model at half filling.

APPENDIX C: SECOND-ORDER SELF-ENERGY AND PHASE-SPACE FACTOR

The result for the second-order retarded self-energy reads [74]

$$\Sigma^r(\omega, \boldsymbol{k}) = U^2 \int d\varepsilon \frac{F^r(\varepsilon, \boldsymbol{k})}{\omega + i\eta - \varepsilon}. \tag{C1}$$

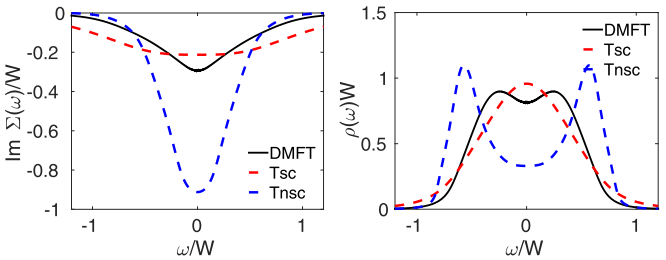

FIG. 15. (Color online) Comparison of DMFT-NRG result with self-consistent (Tsc) and non-self-consistent (Tnsc) T-matrix calculations for $\mathrm{Im}\Sigma(\omega)$ and $\rho(\omega)$ for $U/W = 0.6$ and $T/W = 0.2$.

The imaginary part of the retarded self-energy is then given by

$$\mathrm{Im}\Sigma^r_{\boldsymbol{k}}(\omega) = -\pi U^2 F^r(\omega,\boldsymbol{k}), \tag{C2}$$

where $F^r(\varepsilon,\boldsymbol{k}) = f_1(\varepsilon,\boldsymbol{k}) + f_2(\varepsilon,\boldsymbol{k})$, with the phase-space factors

$$f_1(\varepsilon,\boldsymbol{k}) = \sum_{\boldsymbol{k}_1,\boldsymbol{k}_2,\boldsymbol{k}_3} \delta\big(\xi_{\boldsymbol{k}_2} + \xi_{\boldsymbol{k}_3} - \xi_{\boldsymbol{k}_1} - \varepsilon\big) \times \delta(\boldsymbol{k}+\boldsymbol{k}_1,\boldsymbol{k}_2+\boldsymbol{k}_3) n_{\boldsymbol{k}_1}\big(1-n_{\boldsymbol{k}_2}\big)\big(1-n_{\boldsymbol{k}_3}\big) \tag{C3}$$

and,

$$f_2(\varepsilon,\boldsymbol{k}) = \sum_{\boldsymbol{k}_1,\boldsymbol{k}_2,\boldsymbol{k}_3} \delta\big(\xi_{\boldsymbol{k}_2} + \xi_{\boldsymbol{k}_3} - \xi_{\boldsymbol{k}_1} - \varepsilon\big) \times \delta(\boldsymbol{k}+\boldsymbol{k}_1,\boldsymbol{k}_2+\boldsymbol{k}_3)\big(1-n_{\boldsymbol{k}_1}\big) n_{\boldsymbol{k}_2} n_{\boldsymbol{k}_3}. \tag{C4}$$

The expressions can be simplified in the limit of large dimensions. The momentum integrations can be replaced by integrals over the density of states, momentum conservation is implicit so we can omit the corresponding δ function, and the $\boldsymbol{k}$ dependence disappears:

$$f_1(\varepsilon) = \int \mathrm{d}\varepsilon_1 \int \mathrm{d}\varepsilon_2 \int \mathrm{d}\varepsilon_3 \; \rho_0(\varepsilon_1)\rho_0(\varepsilon_2)\rho_0(\varepsilon_3) \times \delta(\varepsilon_2+\varepsilon_3-\varepsilon_1-\varepsilon-\mu) \times n_{\mathrm{F}}(\varepsilon_1-\mu) n_{\mathrm{F}}(-\varepsilon_2+\mu) n_{\mathrm{F}}(-\varepsilon_3+\mu). \tag{C5}$$

We can do the integration over the δ function:

$$f_1(\varepsilon) = \int \mathrm{d}\varepsilon_2 \int \mathrm{d}\varepsilon_3 \; \rho_0(\varepsilon_2+\varepsilon_3-\varepsilon-\mu) \times \rho_0(\varepsilon_2)\rho_0(\varepsilon_3) n_{\mathrm{F}}(\varepsilon_2+\varepsilon_3-\varepsilon-\mu) \times n_{\mathrm{F}}(-\varepsilon_2+\mu) n_{\mathrm{F}}(-\varepsilon_3+\mu), \tag{C6}$$

and similarly for $f_2(\varepsilon)$. In the particle-hole symmetric case we have

$$f_2(\varepsilon) = f_1(-\varepsilon), \tag{C7}$$

It is then sufficient to evaluate $f_1(\varepsilon)$ and we can write

$$F^r(\varepsilon,\boldsymbol{k}) = F^r(\varepsilon) = f_1(\varepsilon) + f_1(-\varepsilon). \tag{C8}$$

This can be evaluated as a double integral for a given temperature and $\rho_0(\varepsilon)$. Assuming that $\rho_0(\varepsilon)$ is only finite in an interval $(-D,D)$ we can analyze the double integration as being determined by a certain region in the ε_3-ε_2 plane. At $T=0$ a geometric analysis of the integration region shows $f_1(\varepsilon) \sim \varepsilon^2$, which gives the typical Fermi-liquid behavior, Eq. (10), at low temperature. In the opposite limit, $T \to \infty$, a similar analysis shows that $F^r(\varepsilon)$ is maximal at $\varepsilon = 0$ and it decays for small ε as $-\varepsilon^2$, which yields the NFL form Eq. (11). One can estimate the crossover temperature T_{FL} by studying when the coefficient of the ε^2 changes sign. Depending on the density of states and the approximations made one finds a result of the order of a fraction of the bandwidth, consistent with the result in Fig. 2 for small U.

[1] T. Timusk and B. Statt, Rep. Prog. Phys. **62**, 61 (1999).
[2] A. A. Kordyuk, Low Temp. Phys. **41**, 319 (2015).
[3] S. Chakravarty, R. B. Laughlin, D. K. Morr, and C. Nayak, Phys. Rev. B **63**, 094503 (2001).
[4] D. J. Scalapino, Rev. Mod. Phys. **84**, 1383 (2012).
[5] V. Emery and S. Kivelson, Nature (London) **374**, 434 (1995).
[6] V. Mishra, U. Chatterjee, J. C. Campuzano, and M. R. Norman, Nat. Phys. **10**, 357 (2014).
[7] K. Efetov, H. Meier, and C. Pépin, Nature Physics **9**, 442 (2013).
[8] J. Bardeen, L. Cooper, and J. Schrieffer, Phys. Rev. **108**, 1175 (1957).
[9] D. M. Eagles, Phys. Rev. **186**, 456 (1969).
[10] A. J. Leggett, in *Modern Trends in the Theory of Condensed Matter*, edited by A. Pekalski and R. Przystawa (Springer, Berlin, 1980).
[11] P. Nozières and S. Schmitt-Rink, J. Low Temp. Phys. **59**, 195 (1985).
[12] M. Randeria, in *Bose-Einstein Condensation*, edited by A. Griffin, D. Snoke, and S. Strinagari (Cambridge University, Cambridge, 1995).
[13] M. Greiner, C. Regal, and D. Jin, Nature (London) **426**, 537 (2003).
[14] M. W. Zwierlein, C. A. Stan, C. H. Schunck, S. M. F. Raupach, A. J. Kerman, and W. Ketterle, Phys. Rev. Lett. **92**, 120403 (2004).
[15] M. Zwierlein, J. Abo-Shaeer, A. Shirotzek, C. H. Schunck, and W. Ketterle, Nature (London) **435**, 1047 (2005).
[16] I. Bloch, J. Dalibard, and W. Zwerger, Rev. Mod. Phys. **80**, 885 (2008).
[17] J. K. Chin, D. E. Miller, Y. Liu, C. Stan, W. Setiawan, C. Sanner, K. Xu, and W. Ketterle, Nature (London) **443**, 961 (2006).
[18] M. Feld, B. Fröhlich, E. Vogt, M. Koschorreck, and M. Köhl, Nature (London) **480**, 75 (2011).
[19] J. Gaebler, J. Stewart, T. Drake, D. Jin, A. Perali, P. Pieri, and G. Strinati, Nature Physics **6**, 569 (2010).
[20] M. Randeria, Nature Physics **6**, 561 (2010).
[21] E. V. Doggen and J. J. Kinnunen, Scientific Reports **5**, 9539 (2015).
[22] Q. Chen, K. Levin, and J. Stajic, J. Low Temp. Phys. **32**, 406 (2006).
[23] T. Eckl, D. J. Scalapino, E. Arrigoni, and W. Hanke, Phys. Rev. B **66**, 140510 (2002).
[24] A. Georges, G. Kotliar, W. Krauth, and M. Rozenberg, Rev. Mod. Phys. **68**, 13 (1996).
[25] Q. Chen, J. Stajic, S. Tan, and K. Levin, Phys. Rep. **412**, 1 (2005).
[26] C.-C. Chien, H. Guo, Y. He, and K. Levin, Phys. Rev. A **81**, 023622 (2010).
[27] M. Keller, W. Metzner, and U. Schollwöck, Phys. Rev. B **60**, 3499 (1999).
[28] D. Rohe and W. Metzner, Phys. Rev. B **63**, 224509 (2001).
[29] F. Marsiglio, P. Pieri, A. Perali, F. Palestini, and G. C. Strinati, Phys. Rev. B **91**, 054509 (2015).
[30] A. Perali, P. Pieri, G. C. Strinati, and C. Castellani, Phys. Rev. B **66**, 024510 (2002).
[31] S. Tsuchiya, R. Watanabe, and Y. Ohashi, Phys. Rev. A **80**, 033613 (2009).

[32] R. Watanabe, S. Tsuchiya, and Y. Ohashi, Phys. Rev. A **82**, 043630 (2010).
[33] R. Haussmann, Z. Phys. B **91**, 291 (1992).
[34] R. Haussmann, M. Punk, and W. Zwerger, Phys. Rev. A **80**, 063612 (2009).
[35] M. Bauer, M. M. Parish, and T. Enss, Phys. Rev. Lett. **112**, 135302 (2014).
[36] P. Magierski, G. Wlazłowski, A. Bulgac, and J. E. Drut, Phys. Rev. Lett. **103**, 210403 (2009).
[37] H. Hu, X.-J. Liu, P. D. Drummond, and H. Dong, Phys. Rev. Lett. **104**, 240407 (2010).
[38] G. Wlazłowski, P. Magierski, J. E. Drut, A. Bulgac, and K. J. Roche, Phys. Rev. Lett. **110**, 090401 (2013).
[39] M. Randeria, N. Trivedi, A. Moreo, and R. T. Scalettar, Phys. Rev. Lett. **69**, 2001 (1992).
[40] N. Trivedi and M. Randeria, Phys. Rev. Lett. **75**, 312 (1995).
[41] Y. Vilk and A.-M. Tremblay, J. Phys. I **7**, 1309 (1997).
[42] S. Moukouri, S. Allen, F. Lemay, B. Kyung, D. Poulin, Y. M. Vilk, and A.-M. S. Tremblay, Phys. Rev. B **61**, 7887 (2000).
[43] A. Koga and P. Werner, Phys. Rev. A **84**, 023638 (2011).
[44] A. Koga and P. Werner, Mod. Phys. Lett. B **25**, 973 (2011).
[45] M. Randeria and E. Taylor, Annual Review of Condensed Matter Physics **5**, 209 (2014).
[46] B. Kyung, S. Allen, and A.-M. S. Tremblay, Phys. Rev. B **64**, 075116 (2001).
[47] M. Keller, W. Metzner, and U. Schollwöck, Phys. Rev. Lett. **86**, 4612 (2001).
[48] M. Capone, C. Castellani, and M. Grilli, Phys. Rev. Lett. **88**, 126403 (2002).
[49] B. Kyung, A. Georges, and A.-M. S. Tremblay, Phys. Rev. B **74**, 024501 (2006).
[50] N. Kuleeva, E. Kuchinskii, and M. Sadovskii, J. Exp. Theor. Phys. **119**, 264 (2014).
[51] A. Garg, H. R. Krishnamurthy, and M. Randeria, Phys. Rev. B **72**, 024517 (2005).
[52] A. Toschi, P. Barone, M. Capone, and C. Castellani, New J. Phys. **7**, 7 (2005).
[53] A. Toschi, M. Capone, and C. Castellani, Phys. Rev. B **72**, 235118 (2005).
[54] J. Bauer and A. C. Hewson, Europhys. Lett. **85**, 27001 (2009).
[55] J. Bauer, A. C. Hewson, and N. Dupuis, Phys. Rev. B **79**, 214518 (2009).
[56] R. Micnas, J. Ranninger, and S. Robaszkiewicz, Rev. Mod. Phys. **62**, 113 (1990).
[57] R. Micnas, S. Robaszkiewicz, and T. Kostyrko, Phys. Rev. B **52**, 6863 (1995).
[58] S. Robaszkiewicz, R. Micnas, and K. A. Chao, Phys. Rev. B **23**, 1447 (1981).
[59] R. Micnas and T. Kostyrko, in *Recent Developments in High Temperature Superconductivity*, Lecture Notes in Physics Vol. 475, edited by J. Klamut, B. Veal, B. Dabrowski, and P. Klamut (Springer, Berlin, 1996), pp. 221–242.
[60] A. Cichy and R. Micnas, Annals of Physics **347**, 207 (2014).
[61] R. Bulla, T. Costi, and T. Pruschke, Rev. Mod. Phys. **80**, 395 (2008).
[62] R. Peters, T. Pruschke, and F. B. Anders, Phys. Rev. B **74**, 245114 (2006).
[63] A. Weichselbaum and J. von Delft, Phys. Rev. Lett. **99**, 076402 (2007).
[64] R. Bulla, T. A. Costi, and D. Vollhardt, Phys. Rev. B **64**, 045103 (2001).
[65] A. Georges, Annalen der Physik **523**, 672 (2011).
[66] We would like to thank N. Dupuis for pointing this out to us.
[67] L. De Leo, J.-S. Bernier, C. Kollath, A. Georges, and V. W. Scarola, Phys. Rev. A **83**, 023606 (2011).
[68] E. Khatami, E. Perepelitsky, M. Rigol, and B. S. Shastry, Phys. Rev. E **89**, 063301 (2014).
[69] We use this as a general condition also at finite temperature, even though the Fermi surface is strictly only defined at $T = 0$.
[70] A. Kampf and J. R. Schrieffer, Phys. Rev. B **41**, 6399 (1990).
[71] A. P. Kampf and J. R. Schrieffer, Phys. Rev. B **42**, 7967 (1990).
[72] J. Bauer and M. Babadi (unpublished).
[73] J. Bauer and A. C. Hewson, Eur. Phys. J. B **57**, 235 (2007).
[74] H. Schweitzer and G. Czycholl, Z. Phys. B **83**, 93 (1991).